CFD SIMULATION OF A TRANSONIC AXIAL-FLOW COMPRESSOR STAGE

Alessandro Cassolari Vaz da Silva, alessandrocvs@lasme.coppe.ufrj.br
Universidade Federal do Rio de Janeiro, COPPE, Nuclear Engineering Program

Newton R. Moura, newton.moura@petrobras.com.br
Petrobras/CENPES/Gas and Energy

Jian Su, sujian@lasme.coppe.ufrj.br
Universidade Federal do Rio de Janeiro, COPPE, Nuclear Engineering Program

Abstract. *Computational simulation of turbulent flow in the rotor-stator stage of an actual transonic axial-flow compressor was performed. A methodology is described for steady state flow simulation of the compressor stage, which include the tip gap between rotor blade and shroud. The turbulence model utilized was SST available in ANSYS CFX 12.0, which was chosen since it combines the k-e and k-w models by applying each one where they have the best performance.*

Keywords: *turbomachinery; CFD; axial flow compressor; SST*

1. INTRODUCTION

Axial flow compressors produce a continuous flux of compressed gas, and have the benefits of high efficiencies and large mass flow capacity, particularly in relation to their cross-section. However, they do require several rows of airfoils to achieve large pressure rises making them complex and expensive relative to other designs. Axial compressors are widely used in gas turbines, such as jet engines and small scale power stations.

Computational Fluid Dynamics (CFD) has been extensively used to analyze the flow through rotating machineries in general and through axial compressors particularly (Belamri et al., 2005a,b, Denton and Dawes, 1999, Hall, 1998a,b, Wu et al., 2005, Xu and Chen, 2005). Due to the high cost of the experiment in this area, CFD codes have become an excellent tool for analysis and design of turbomachinery. Hall (1998a,b) investigated improved numerical techniques for predicting flows through multistage compressors, using the Pennsylvania State University Research Compressor (PSRC) as a test case. Several computational fluid dynamics techniques were applied to predict both steady and unsteady flows through the PSRC facility. Interblade row coupling via a circumferentially averaged mixing-plane approach was employed for steady flow analysis. Belamri et al. (2005a,b) analyzed the flow flied of a 15-stage Siemens V84.3A axial compressor using the CFD code CFX-5. They concluded that accurate predictions of the overall performance including pressure rise and efficiency could be obtained by using a single passage steady state (*Stage*) model with reasonable meshes and computing resources. Wu et al. (2005) presented a large-scale acroelasticity computation for an acro-engine core compressor with 17 bladerows, using a mesh with over 68 million points. The Favre-averaged Navier-Stokes equations were used to represent the flow in a non-linear time-accurate fashion on unstructured meshes of mixed elements. A comparison of the averaged unsteady flow and the steady-state flow revealed some discrepancies.

The report presented by Simões et al. (2009) shows a study of a computational fluid dynamics tool (CFD) in the evaluation of the turbulent flow inside a transonic axial compressor rotor named NASA 37. Three available turbulence models were tested and validated against experimental data. The selected models, all being two-equation type, are standard $\kappa - \epsilon$, $\kappa - \omega$ and SST. It was concluded that the SST turbulence model was validated for this problem by presenting the most accurate results among the three evaluated models and the smallest absolute error percentage estimated in the design point around $4,02\%$. The turbulence model $\kappa - \omega$ did not achieve precise solutions for this flow type and the $\kappa - \epsilon$ model reached slightly worse results than the ones obtained with the SST model.

This paper describes the application of the commercial CFD code CFX 12.0 to model the complete flow field of the first stage axial compressor. The aim of this study is to analyze the interaction between rotor-stator components as well as the differences in the solution due to the change of the interface model.

2. GEOMETRY AND MESHING

The geometry of this stage was obtained by 3D scanning of an actual compressor of a gas turbine used for power generation. Each modeled blade was repeated in the tangential direction according to the number of blades of each component existing in the real machine. Figure 1 shows the geometry used. The mesh was generated using all hex elements, employing an H mesh topology, O-grid around the blade surface and hex element in the tip region. A fine mesh of approximately 500k nodes per component (a total of 1,5 million nodes) was used.

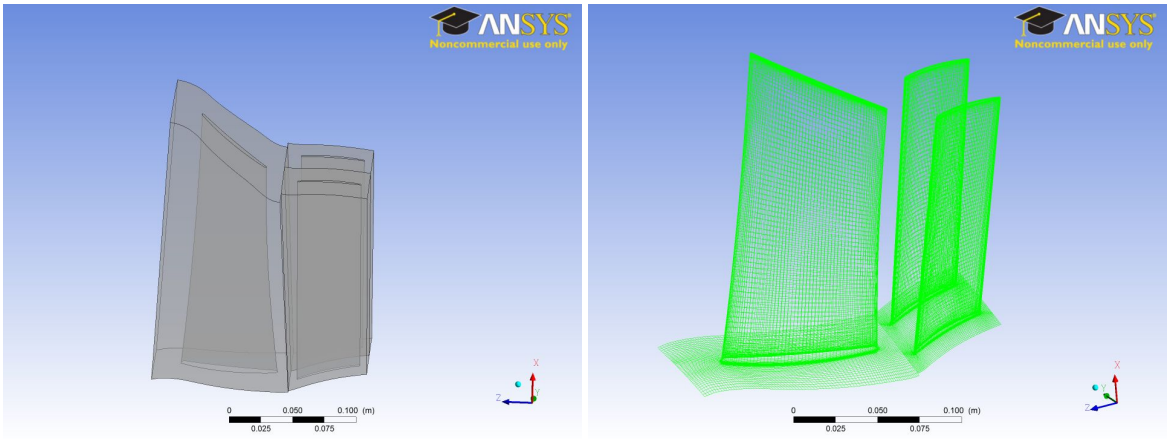

Figure 1. Compressor stage geometry and mesh.

3. MATHEMATICAL MODELING

For the mathematical model, it was considered three dimensional, transient, turbulent flow of a Newtonian fluid with constant thermophysical properties. The continuity equation is:

$$\frac{\partial \rho}{\partial t} + \nabla \bullet (\rho U) = 0 \tag{1}$$

in which ρ is the specific mass, U is the velocity vector and t is the time. The Reynolds averaged Navier-Stokes (RANS) equations are given by:

$$\frac{\partial \rho U}{\partial t} + \nabla \bullet (\rho U \otimes U) - \nabla \bullet (\mu_{eff} \nabla U) = \nabla p^{'} + \nabla \bullet (\mu_{eff} \nabla U)^T + B \tag{2}$$

in which μ_{eff} is the effective viscosity, $p^{'}$ is the turbulent modified pressure and B is the body force vector. For this study, B is defined as:

$$B = S_{Cor} + S_{cfg} \tag{3}$$

In which:

$$S_{Cor} = -2\rho\omega \times U \tag{4}$$

$$S_{cfg} = -\rho\omega \times (\omega \times r) \tag{5}$$

and in which r is the location vector.

The turbulent modified pressure is defined by:

$$p^{'} = p + \frac{2}{3}\rho k \tag{6}$$

in which p is pressure, k is turbulence kinetic energy.

The effective viscosity is given by:

$$\mu_{eff} = \mu + \mu_t \tag{7}$$

In this research, the SST turbulence model - $ShearStressTransport$ Menter (1997), Menter et al. (2003) was employed, which was indicated for calculation of skin friction and heat flow at solid surface. This model uses the k - ω near the wall and the k - ϵ far from the wall, where each one gives better results.

The transformed equations for the k - ϵ and the k - ω for SST turbulence model are:

$$\frac{\partial(\rho k)}{\partial t} + \nabla \bullet (\rho \mathbf{U} k) = \nabla \bullet \mu + \mu_t \sigma_k \nabla k + \widetilde{P}_k - \beta^* \rho \omega k \tag{8}$$

$$\frac{\partial \rho\omega}{\partial t} + \nabla \bullet \rho \mathbf{U} \omega = \nabla \bullet \mu + \mu_t \sigma_\omega \nabla \omega + 2(1 - F_1)\rho\sigma_{\omega 2}\frac{1}{\omega}\nabla k \bullet \nabla\omega + \frac{\alpha}{\nu_t}P_k - \beta\rho\omega^2 \tag{9}$$

in which ω is the turbulence frequency and $\nu_t = \mu_t/\rho.P_k$ is the shear production of turbulence and its limits are defined by:

$$P_k = \tau : \nabla \mathbf{U} \quad \rightarrow \quad \widetilde{P}_k = \min(P_k, 10\beta^* \rho k \omega) \tag{10}$$

in which the Reynolds stress tensor is given by $\tau = 2\mu_t \mathbf{D} - \frac{2}{3}\rho k \delta$, where $\mathbf{D} = \frac{1}{2}\nabla \mathbf{U} + \nabla \mathbf{U}^T$.

All the model constants are obtained by combination of the corresponding constants of the $k-\epsilon$ and $k-\omega$ model using a blending function F_1 by $\alpha = \alpha_1 F_1 + \alpha_2(1 - F_1)$, where α_1 e α_2 are constants of the models $k-\omega$ and $k-\epsilon$ respectively.

The constants for this model are: $\beta^* = 0,09$, $\alpha_1 = 5/9$, $\beta_1 = 3/40$, $\sigma_{kl} = 0,85$, $\sigma_{\omega l} = 0,5$, $\alpha_2 = 0,44$, $\beta_2 = 0,0828$, $\sigma_{k2} = 1$ e $\sigma_{\omega 2} = 0,856$.

The first blending function F_1 is defined by:

$$F_1 = \tanh\left\{\left\{\min\left[\max\left(\frac{\sqrt{k}}{\beta^* \omega y}, \frac{500\nu}{y^2\omega}\right), \frac{4\rho\sigma_{\omega 2} k}{CD_{k\omega} y^2}\right]\right\}^4\right\} \tag{11}$$

in which $CD_{k\omega}$ is

$$CD_{k\omega} = \max\left(2\rho\sigma_{\omega 2}\frac{1}{\omega}\nabla k \bullet \nabla\omega, 10^{-10}\right) \tag{12}$$

and y is the distance to the nearest wall.

F_1 is equal to zero away from the surface ($k-\epsilon$ model), and switches to one inside the boundary layer ($k-\omega$ model). The turbulent eddy viscosity is defined as:

$$\nu_t = \frac{a_1 k}{\max(\quad a_1\omega, SF_2)} \tag{13}$$

in which $a_1 = 0,31$, S is the invariant measure of strain rate given by $\sqrt{2\mathbf{D} : \mathbf{D}}$ and F_2 is a second blending function defined by:

$$F_2 = \tanh\left[\left[\max\left(\frac{2\sqrt{k}}{\beta^*\omega y}, \frac{500\nu}{y^2\omega}\right)\right]^2\right] \tag{14}$$

This model requires the knowledge of the distance between the nodes and the nearest wall. So, a better interaction between the $k-\omega$ and $k-\epsilon$ is obtained. The wall scale equation is solved to get these wall distances:

$$\nabla^2\phi = -1 \tag{15}$$

in which ϕ is the value of the wall scale. The wall distance can be calculated from the wall through:

$$WD = \sqrt{|\nabla\phi|^2 + 2\phi} - |\nabla\phi| \tag{16}$$

The mathematical model was solved numerically by using the commercial CFD package *ANSYS CFX-12.0*. This program employs numerical method of finite volume as solution (Element Based Finite Volume Method - EBFVM), which allows the solution of problems by blending of unstructured grids. Hence, it is possible to obtain a numerical solution of discretized momentum and mass balance equations.

4. BOUNDARY CONDITIONS

At the design conditions, the compressor rotates at approximately 3627 rpm, delivering $131,55kg/s$ of air. An ideal gas approximation is applied for air. One blade passage per component is modeled. A total pressure and direction profile is specified at the inlet, and a mass flow rate is specified at the outlet. Due to the instability of the convergence we used a ramp to mass flow, causing it to vary slowly in relation to the number of iterations until it reaches its true value, as shown in figure 2. Connections between rotating and stationary components are made using two distinct interface model, stage and frozen rotor interfaces. The turbulence is modeled using the SST model. The time step used to obtain the stead state simulation was 0.0002 sec, corresponding to $0.1/omega\ [rad/sec]$.

5. INTERFACE MODELS

Three frame change interfaces are avaiable in ANSYS CFX 12.0: *Stage*, *Frozen Rotor*, and *Transient Rotor-Stator*. The last model was not used since only a steady state flow was considered in this work.

In the *Frozen Rotor* model the frame of reference and/or pitch is changed but the relative orientation of the components across the interface is fixed. The two frames of reference connect in such a way that each of them have a fixed relative position throughout the calculation. If the frame changes the appropriate equation transformations are made. If the pitch changes, the fluxes are scaled by the pitch change. This can be observed in figure 3. The difference of pressure profile in the rotor to stator interface is not very large in this simulation as the rotor pitch change is close to stator pitch change.

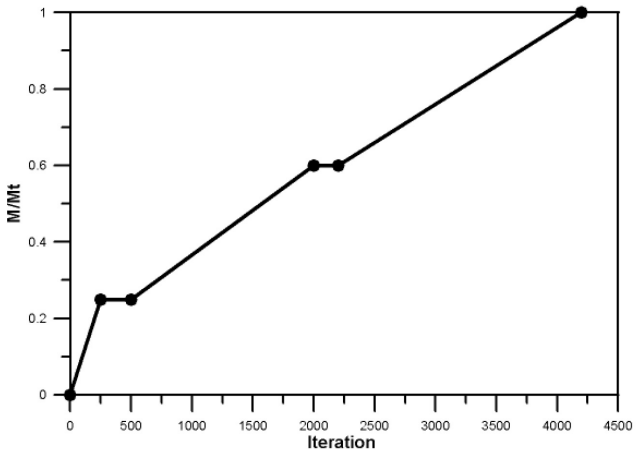

Figure 2. Function used for mass flow ramp.

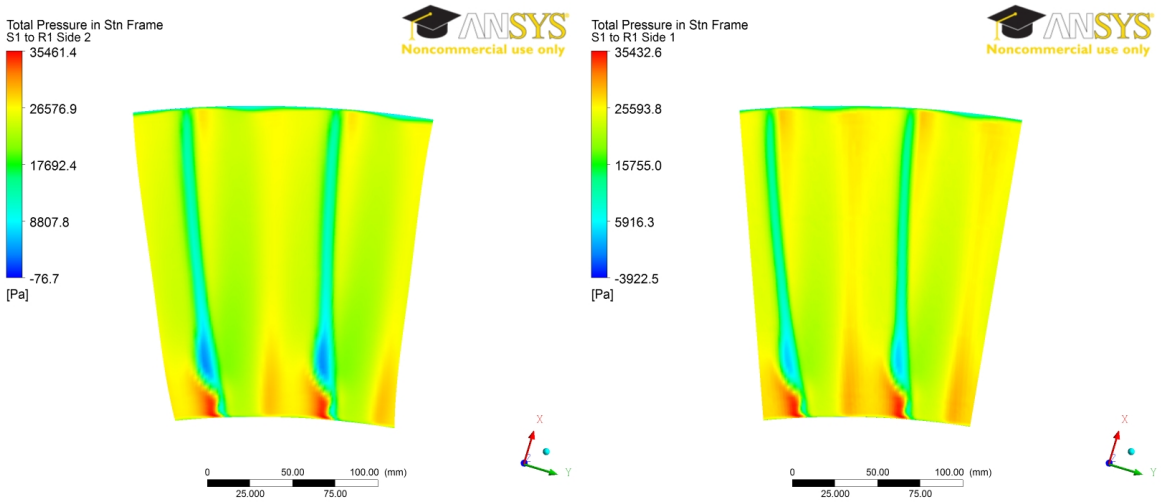

Figure 3. Predicted total pressure calculated by the frozen rotor model at rotor and stator interfaces, respectively.

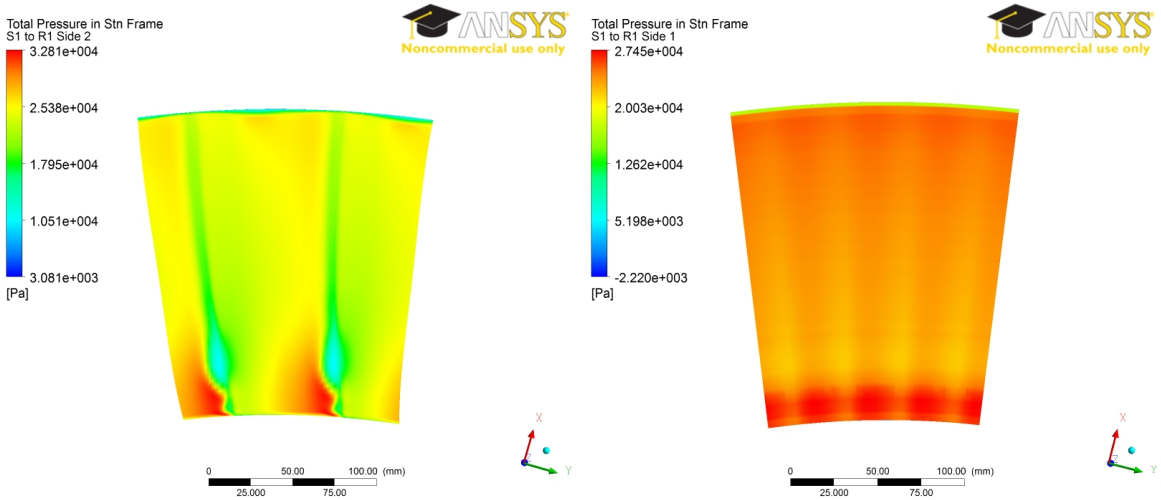

Figure 4. Predicted total pressure calculated by the stage model at rotor and stator interfaces, respectively.

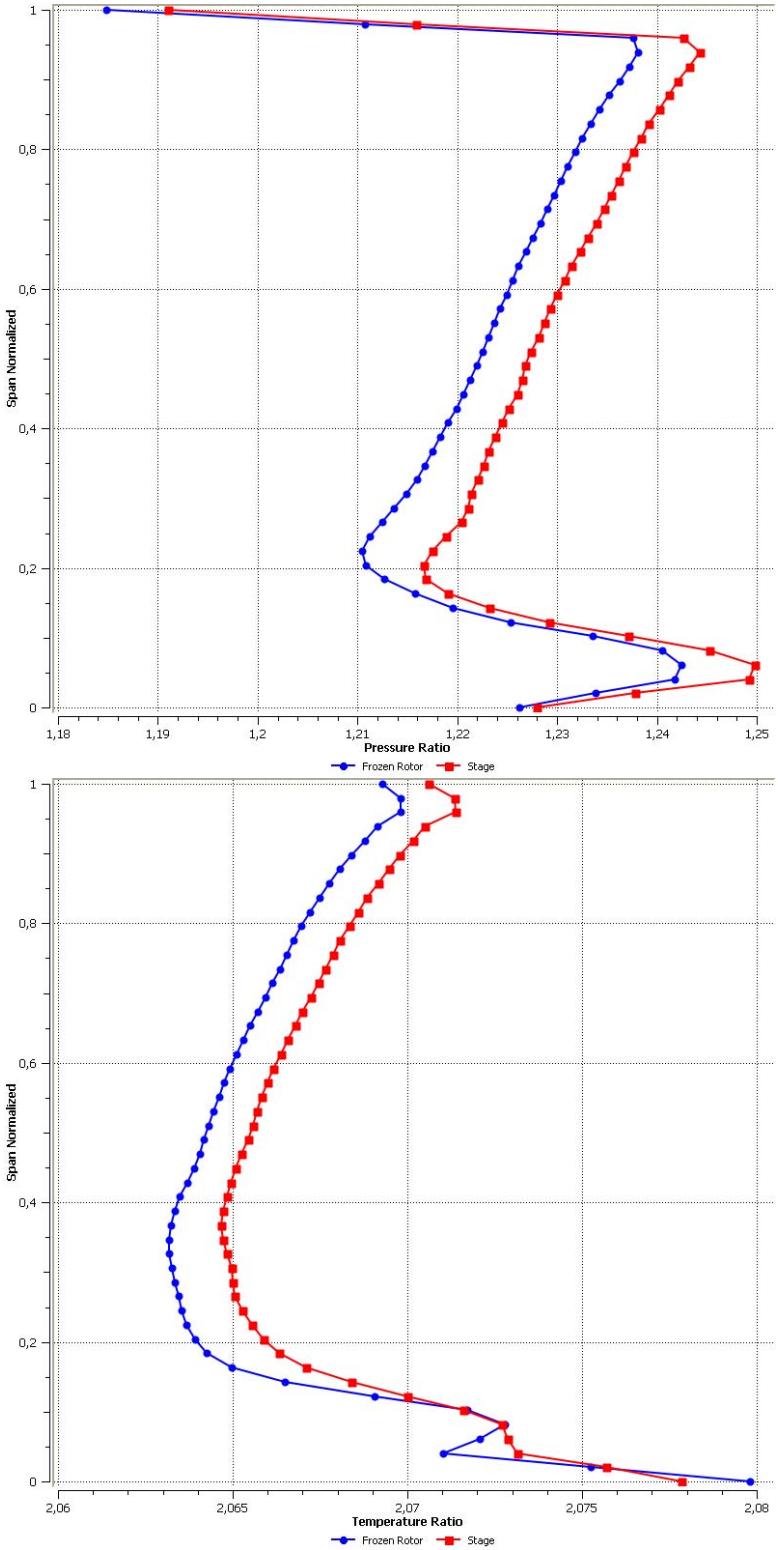

Figure 5. Pressure ratio and temperature ratio as function of span location.

The *Stage* model is an alternative to *Frozen Rotor* for modeling frame and/or pitch change. Instead of assuming a fixed relative position of the components, the stage model performs a circumferential averaging of the fluxes through bands on the interface. Figure 4 shows this circumferential averaging at stator interface. Steady state solutions are then obtained in each reference frame. The stage averaging at the frame change interface incurs a one-time mixing loss, which makes it equivalent to assume that the physical mixing supplied by the relative motion between components is sufficiently large to cause any upstream velocity profile to mix out prior to entering the downstream machine component.

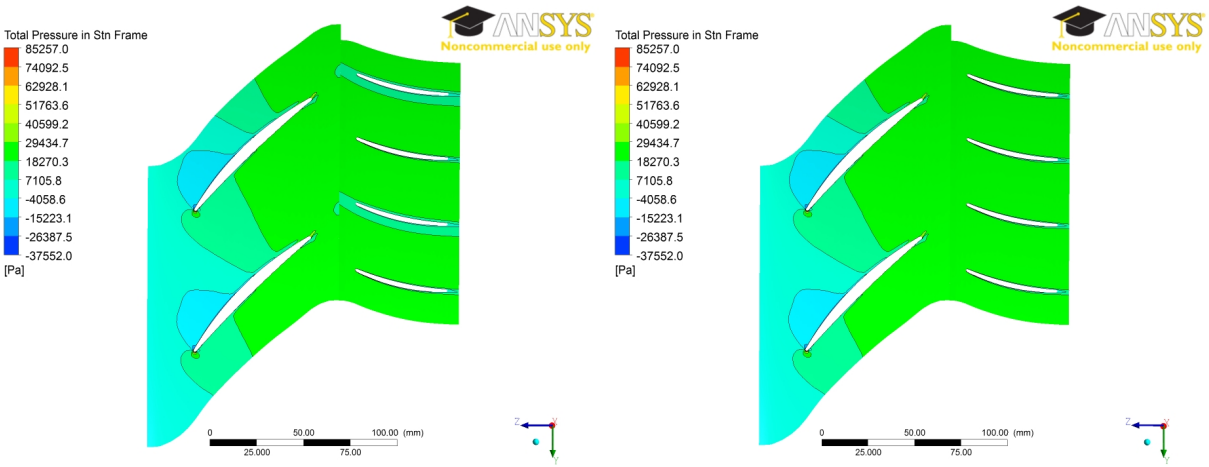

Figure 6. Predicted total pressure calculated by the frozen rotor and stage models, respectively.

A study was conducted to analyze the influence of interface models in the results. Figure 5 shows the pressure ratio and temperature ratio as function of span location in the middle of the stator. We can notice that the error caused due the change of interface model is less than 1% for both pressure and temperature ratios.

Figure 6 shows the predicted total pressure calculated by both interface models. We can observe a small difference in a stator when we use the *Frozen Rotor* model. This difference is because the *Frozen Rotor model* scales the fluxes by the pitch change, thus having no symmetry in the tangential direction. In the Stage model, due to the circumferential average, there is symmetry in the tangential direction causing the predicted total pressure to be equal on all stators.

6. RESULTS

Table 1 shows some performance results of both interface models. We can observe that the difference in results is not great. This can be explained by the fact that the circumferential variation of the flow is of the order of the component pitch, and also because the interface of the rotor and stator have similar areas, enabling the application of both models.

In figure 7 (a) it is possible to observe one of the most important phenomena in transonic axial compressors which is normal shock wave. It begins upstream of the blade and reaches the suction face of the following blade at about 80% of the chord. This is responsible for the increase of pressure in the compressor rotor, as shown in Figure 7 (b). After this shock wave the flow becomes subsonic and there is a large increase in the entropy of the system.

In figure 7 (b) the typical predicted total pressure is illustrated at mid span of the passage. The pressure increases smoothly from the inlet to outlet to reach the desired design pressure ratio. To achieve the design pressure ratio, the compressor requires a high mass flow rate, which is limited by the mechanical stresses, operating range and stage efficiency.

Figure 7 (c) shows the velocity vectors in the compressor stage. As boundary condition, the flow enters the rotor perpendicular to the inlet face. The flow is then deflected by the rotor and corrected by the stator to enter the downstream stage with the desired direction. The stator, besides correcting the direction of flow, acts as a diffuser giving a small increase in pressure. However, as noted earlier, the biggest increase in pressure occurs in the rotor due to shock waves.

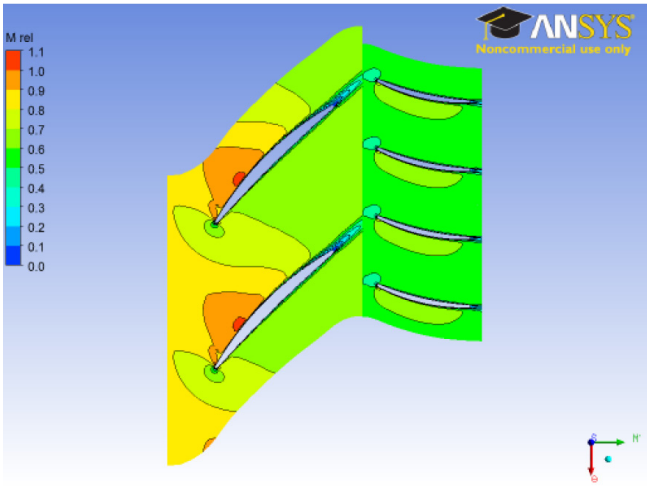

(a)

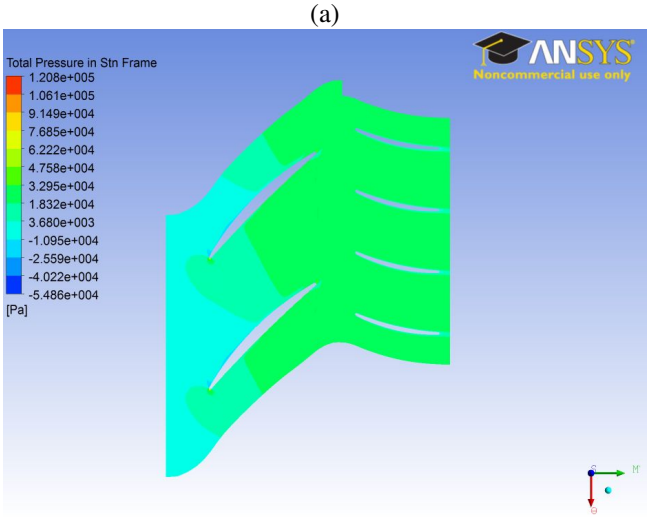

(b)

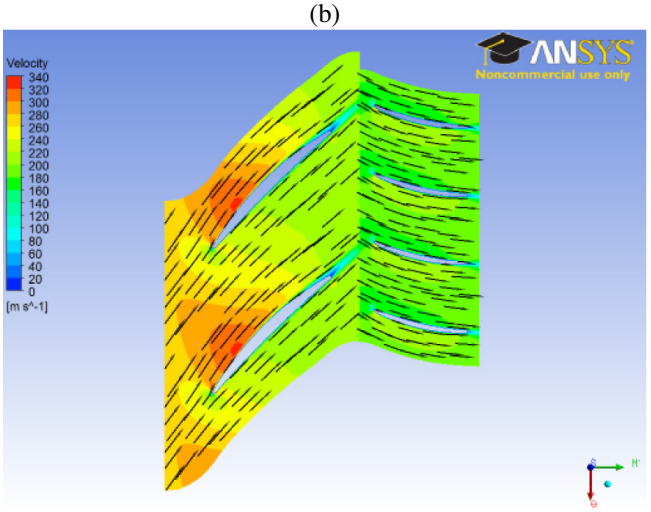

(c)

Figure 7. (a) Relative mach number contour, (b) total pressure contour, and (c) stage velocity vectors at 50% span

Table 1. Stage performance results.

	Stage	Frozen Rotor
Rotation Speed	3627 rpm	3627 rpm
Inlet Mass Flow Rate	131.5520 Kg/s	131.55
Inlet Volume Flow Rate	106.1270 m^3/s	106.1260 m^3/s
Input Power	1.64 MW	1.58 MW
Total Pressure Ratio	1.23	1.22
Total Temperature Ratio	1.07	1.07
Total-to-Total Polytropic Efficiency	90.94%	91.56%
Total-to-Total Isentropic Efficiency	90.70%	91.73%

7. CONCLUSIONS

This simulation showed that both interface models provide good results for the understanding of the flow in multistage compressors. However, physical phenomena like recirculations are not transported from one domain to another. To achieve a better study of these phenomena, it would be necessary to analyze transient flow using the interface model transient rotor-stator which would require more time and computational cost. For this study, the *Frozen Rotor* interface model gave a good result because the rotor pitch change is close to the stator pitch change. Nevertheless, in the case of multistage compressors, the *Stage* model is more appropriate. The *Frozen Rotor* model is only used to obtain an initial solution due to its low computational cost.

8. ACKNOWLEDGEMENTS

The authors would like to acknowledge the support of CNPq, CAPES and FAPERJ for the realization of the research. The authors gratefully acknowledge the financial support of Petrobras through Project ANPETRO 11126 and would like to thank Petrobras for the permission to publish the paper.

9. REFERENCES

Belamri, T., Braune, A., Galpin, P., and Cornelius, C. (2005a). Cfd analysis of a 15 stage axial compressor part i: Methods. *ASME Turbo Expo 2005: Power for Land, Sea and Air*.

Belamri, T., Braune, A., Galpin, P., and Cornelius, C. (2005b). Cfd analysis of a 15 stage axial compressor part ii: Results. *ASME Turbo Expo 2005: Power for Land, Sea and Air*.

Denton, J. D. and Dawes, W. N. (1999). Computational fluid dynamics for turbomachinery design. *Proceedings of the Institution of Mechanical Engineers Part C-Journal of Mechanical Engineering Science*, 213(2):107–124.

Hall, E. J. (1998a). Aerodynamic modelling of multistage compressor flow fields part 1: Analysis of rotor-stator-rotor aerodynamic interaction. *Proceedings of the Institution of Mechanical Engineers Part G-Journal of Aerospace Engineering*, 212(G2):77–89.

Hall, E. J. (1998b). Aerodynamic modelling of multistage compressor flow fields part 2: modelling deterministic stresses. *Proceedings of the Institution of Mechanical Engineers Part G-Journal of Aerospace Engineering*, 212(G2):91–107.

Menter, F. R. (1997). Eddy viscosity transport equations and their relation to the k-ϵ model. *Journal of Fluid Engineering*, 119(3):876–884.

Menter, F. R., Kuntz, M., and Langtry, R. (2003). Ten years of industrial experience with the sst turbulence model. *Turbulence, Heat and Mass Transfer 4, Begell House, Inc.*

Simões, M. R., Montojos, B. G., Moura, N. R., and Su, J. (2009). Validation of turbulence models for simulation of axial flow compressor. *20th International Congress of Mechanical Engineering*.

Wu, X., Vahdati, M., Sayma, A., and Imregun, M. (2005). Whole-annulus aeroelasticity analysis of a 17-bladerow wrf compressor using an unstructured navier-stokes solver. *International Journal of Computational Fluid Dynamics*, 19(3):211–223.

Xu, C. and Chen, W. (2005). Computational analysis on a compressor blade. In *Int. Conf. On Jets, Wakes and Separated Flows*, Toba-shi, Mie, Japan.